Strategies for Embedding Optical Fiber Sensors in Additive Manufacturing Structures

Strategies for Embedding Optical Fiber Sensors in Additive Manufacturing Structures

Francesco Falcetelli, Raffaella Di Sante and Enrico Troiani

University of Bologna, Department of Industrial Engineering, Forlì 47121, Italy.
francesco.falcetelli@unibo.it

Abstract. The use of optical fiber sensors (OFS) has spread in the Structural Health Monitoring (SHM) community for their ability to detect many different physical quantities, robustness against electromagnetic disturbances, light weight and embedding possibilities. The last point has been widely investigated for different types of materials, but only recently researchers considered the possibility to embed optical fibers in 3D printed structures. Additive Manufacturing (AM) offers new opportunities in terms of design, for the manufacturing of structures with complex geometries in a relatively low amount of time. However, new challenges must be considered, including innovative embedding solutions for different types of sensors. As a first step, this work discusses current embedding strategies for optical fiber sensors in structures produced with the Fused Deposition Modeling (FDM) technique. A novel methodology to embed OFS is introduced and then tested through the production of specimens at three different filling densities and six different loads. The experimental results, where both distributed OFS and strain gauges were used, were also compared with the data obtained from a numerical model developed in Abaqus/CAE in which the filling pattern of the specimens was accurately reproduced. Finally, the results were critically discussed, highlighting both agreements and discrepancies with respect to the expected data.

Keywords: Optical Fibers, Additive Manufacturing, Embedding Strategies, Structural Health Monitoring

1 Introduction

The concept of Structural Health Monitoring (SHM) consists in the process of implementing a damage evaluation strategy for different engineering structures [1].

Recently, Additive Manufacturing (AM) is emerging as a new technology to produce components characterized by complex geometries, unfeasible with conventional techniques [2]. In the aerospace and automotive sectors, AM technology enables the production of lighter structures maintaining safety [3]. In biomedical applications AM allows the design of structures who resemble the bone configuration and stiffness [4].

Other sectors where AM is getting attention are soft robotics [5], photonics [6] and energy [7].

The integration of sensors within AM components has attracted the attention of several researchers mainly in three main areas of application. First, the realization of different types of sensors where the specific geometry of the AM structures has both protective and transducer functionalities [8]. Second, the monitoring of defects which can potentially occur during the manufacturing process [9, 10]. Third, the monitoring of the critical regions of 3D printed structures during their operational life [11].

In particular, the monitoring of AM structures is challenging for many reasons. Since AM can be considered a layer-oriented technology, the material experiences an anisotropy which is difficult to predict in advance through analytical and numerical modeling. This triggers the need of a meticulous control of several parameters during the manufacturing process. At the same time, the scientific community is making huge efforts to develop measurement protocols to qualify these structures and monitor their integrity [12]. Among the different techniques that can be used for this purpose, Optical Fiber Sensors (OFS) are excellent candidates due to their low size and embedding capabilities, already exploited in other materials such as composites [13, 14].

However, sensor integration into AM structures is still in a preliminary stage and further research is still needed to bring these embedding techniques towards a more mature technology readiness level. The uncertainty on the strain distribution due to the difficulty of positioning the fiber in the correct location represents one open challenge. For example, when the filling density is lower than 100% (i.e. a certain filling pattern is applied) there is a periodical strain distribution along the fiber due to the presence of voids along the path [8]. Indeed, the type of selected filling patterns such as triangles, lines, cubes, etc. determines the frequency and therefore the periodicity of the strain peaks occurring along the fiber.

As a result, the manual positioning of the fiber introduces uncertainty in the measurement system depending on its reciprocal position with respect the filling pattern. Despite this problem, it is a common practice to pause the process and perform the embedding manually [9, 10, 15]. One possibility to overcome this problem is to design a dedicated channel for the fiber. The printing process is paused just after the creation of the channel and then the optical fiber is manually positioned inside of it. The adhesion between the optical fiber and the host structure is crucial to obtain a proper strain transfer [16]. Moreover, often the elastic module of AM structures is low compared with the module of the optical fiber, leading to poor strain transfer capabilities. The Fused Deposition Modeling (FDM) technology offers the possibility to directly deposit the fused material over the fiber. Indeed, some studies exploit this possibility directly resuming the printing process after the positioning of the fiber along the channel [17]. This method ensures a direct strain transfer between the 3D printed material and the fiber, which however is inhomogeneous, with a periodicity determined by the filling density and other design parameters. Therefore, in some cases the use of an intermediary adhesive layer made of epoxy resin or similar adhesives is the preferred choice [18]. Referring to the analytical model developed by the authors in a recent study [19], the strain transfer efficiency, which can be summarized with the shear lag constant value, should decrease due to the presence of the additional layer.

However, in this specific case the improvement of the mechanical coupling between the OFS and the structure, due to the presence of an adhesive layer, compensates the previous effect and can actually increase the shear lag constant, thus accelerating the strain transfer from the structure towards the fiber core. Moreover, the measurement is more stable, since the peak broadening of the reflected spectrum is reduced, and therefore the spatial resolution improved due to the presence of strain gradients along the fiber [20].

However, pausing the printing process is not always possible and increases the time required to produce a component. Another limitation of this approach is that the channel must lay on a plane parallel to the printing plane. Moreover, if the temperature during the manufacturing process exceeds a certain limit, the OFS could be severely damaged.

The aim of this work is to derive an embedding methodology for optical fiber sensors into AM structures to overcome some of the current limitations.

2 Methodology

In this study the FDM technique was considered and the applied methodology is schematized in Fig. 1.

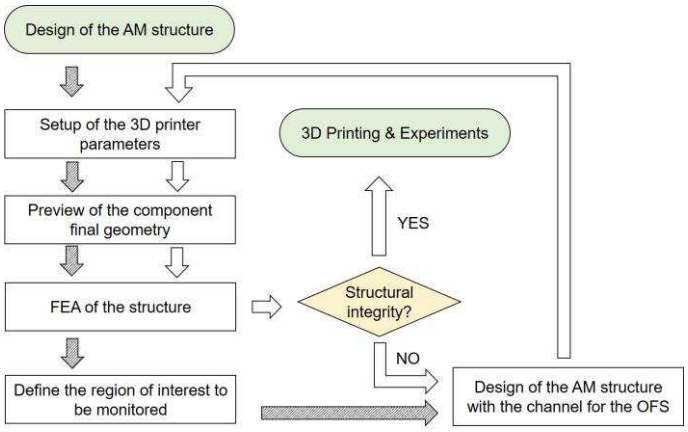

Fig. 1. Flowchart for the embedding methodology for the OFS inside the AM structure

2.1 3D Printer Setup

The first step consisted in the design of the component. In this work, a dog-bone specimen was selected as test structure. Since this is a preliminary study, the aim of this choice was to select a relatively simple structure which could be tested in the following steps. The specimen was designed using SolidWorks^{TM} with an overall length and width of 170 mm and 45 mm respectively, a useful gage length and width of 65 mm and 20 mm respectively and a thickness of 6 mm.

The file was exported in the STL format, required for the 3D printing preprocessing. In particular, the open-source software Ultimaker Cura™ was used since it is widely known in the AM community. Three different specimens having filling densities of 40%, 70% and 100% were considered. Among the various available filling options, the "triangles pattern" was selected because it is relatively simple to model. However, this choice does not compromise the generality of the proposed methodology. Indeed, even if the filling pattern is particularly complex, it is always possible to exploit the information present inside the G-code and develop a numerical model with the desired level of accuracy. When the configuration is completed, the specimen preview is generated, allowing the user to check the actual geometry of the component layer by layer.

2.2 Numerical modelling

The numerical model of the specimen was created using Abaqus/CAE™. The application of Finite Element Analysis (FEA) to AM structures is challenging and the computational cost can grow dramatically if every single detail of the structure is considered. One possibility is to use a nested sub-modeling approach where the inner sub models cover the region of interest to be studied and contain the highest level of details [21]. Nevertheless, in this numerical model the material has been treated as homogenous. Such simplification implies that the stress concentrations at the interface between two adjacent layers are neglected. However, this level of detail is sufficient to evaluate the strain transfer of the OFS, which is the aim of work. To reproduce the actual geometry of the specimens for every case study, a specific script was developed in Python. The use of a specific Python code resulted in a parametric and flexible model in which the shape of every elementary triangle cell could be modified to reproduce the right geometry with the proper filling density. As outlined in Fig. 1, a preliminary numerical analysis was made to obtain a reference with respect to the case where the geometry is modified to incorporate the OFS. The region to be monitored in this case is the central area along the main axis of the specimen. The next step consisted in the modification of the geometry to include a channel for the OFS. A schematic of the specimen with the channel design and its corresponding numerical model are represented in Fig. 2 (a) and Fig. 2 (b) respectively. The groove was created in the central region of the specimen to allow the fiber monitoring of the axial strains, and bends towards the left-hand side in order to avoid the clamping regions. Indeed, the rise of transversal stresses in that area may cause the so-called peak splitting phenomenon [22]. Moreover, this choice offers the possibility to test the embedding of OFS in a channel with a non-trivial straight geometry.

As illustrated in Fig. 1, the previous steps are repeated and finally the FEA of the updated geometry is carried out to verify if the structural integrity is not jeopardized by the presence of the channel.

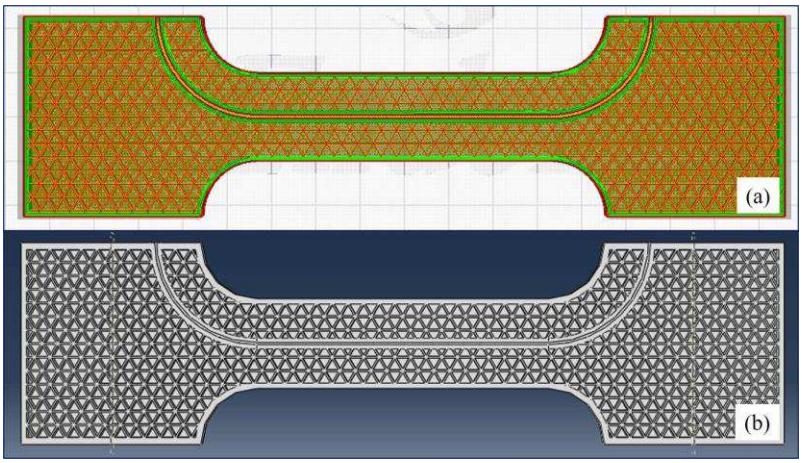

Fig. 2. Preview of the specimen (a), and its numerical modelling with Abaqus/CAE™.

This preliminary result is outlined in Fig. 3. The presence of the channel does not generate any stress concentration but, on the contrary, its structure seems to unload the specimen along the longitudinal direction.

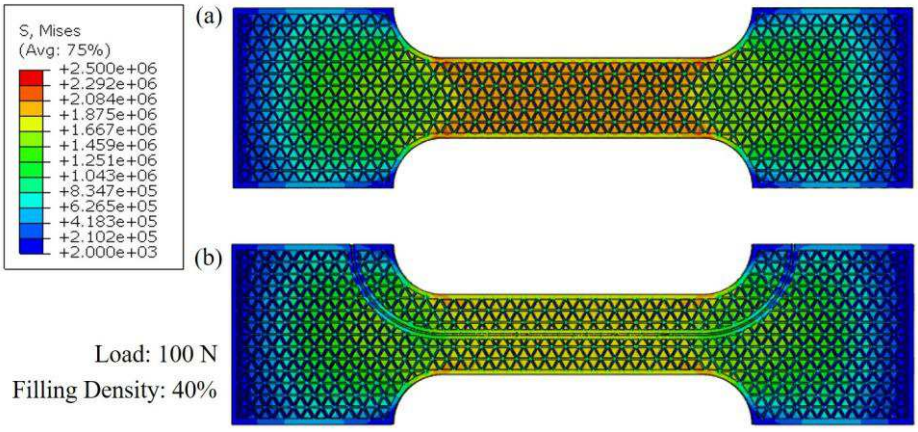

Fig. 3. Comparison of a tensile test simulation at 100N without the channel (a), and with the channel (b), using Abaqus/CAE™.

2.3 Experimental setup

Once the specimen design and numerical modeling were completed, the specimen could be printed and tested. The FDM technique was adopted and the filament of material used was polylactide (PLA). The OFS was firstly inserted inside the channel without any adhesive, in order to reduce friction. One end of the OFS, left over from the specimen, was soaked in the epoxy resin. Then the OFS was pulled inside the

specimen from the opposite end, dragging the resin inside. The used OFS is a SMF-28® from Corning® with a coating diameter of 0.24 mm [23]. Since the fiber is embedded inside the specimen at the end of the process, the channel size must be large enough to guarantee the passage of the OFS. Moreover, due to the possible presence of imperfections which can potentially obstruct the channel, a certain tolerance must be provided. Therefore, after a preliminary experimental campaign to investigate the best channel diameter, a final value of 0.5 mm was selected.

Six load cases were considered for each of the three printed specimens. The strain values were measured using the Optical Backscatter Reflectometer OBR 4413 from Luna Technologies and compared with the strain measured by a strain gauge (SG).

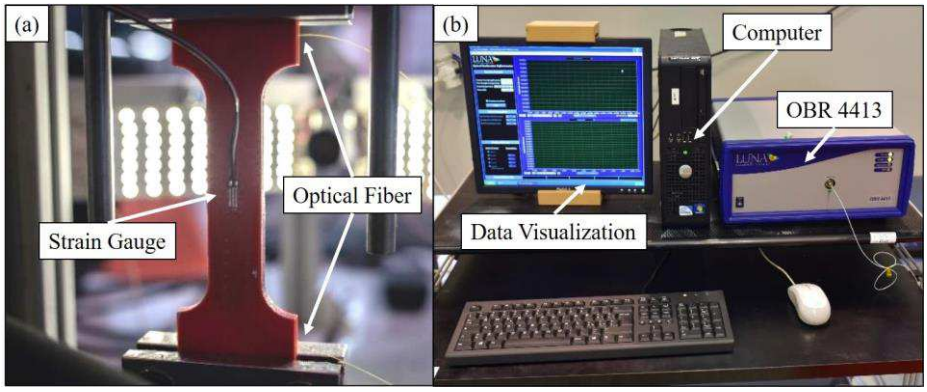

Fig. 4. Specimen during the tensile test (a), and data acquisition system with the OBR 4413 (b).

3 Results and Discussion

The experimental results are summarized in Fig. 5, where the maximum level of strain in each specimen (40%, 70% and 100% of filling density) is represented as a function of the applied load. As expected, the slope relative to the different cases increases for lower filling densities since the structure stiffness decreases. The plot shows a clear linearity in the response both for the SG and the OFS, proving the consistency of the applied methodology. The y-axis on the right-hand side highlights the percentage difference between measurements obtained from the SG and the OFS. For all the three tested configurations the percentage difference decreases with the applied load. This behavior suggests that the coupling between the OFS, the adhesive and the channel in the structure is load-dependent. As a matter of fact, it is challenging to create a uniform bonding layer inside the channel and there is even the possibility that in some regions the fiber loses contact with the host structure. When the load increases, the specimen is stretched along its axial direction and the diameter of the channel decreases due to the Poisson effect. In the regions where the bonding is not perfect the mechanical coupling is guaranteed only by friction which increases with the applied load for the above mentioned reason, explaining the behavior of Fig. 5. This effect,

which is common to all the configurations, is slightly more pronounced in the 40% filling density scenario, with a percentage difference decrease of 5% against the 4% of the other two cases. On the other hand, the absolute value of the percentage difference is similar for the 70% and 100% configurations, and significantly lower for the 40% case. Even if further investigation is needed to fully understand this behavior, the authors believe that the channel restriction caused by the applied load is significantly higher when the filling density is low, resulting in a more efficient strain transfer.
Since the OBR 4413 performs distributed sensing, it is interesting to analyze also the overall strain distribution along the fiber rather than only the maximum value (see Fig. 6). In the figure, the different regions of the channel are delimited by the vertical dashed lines. The maximum value is found in the central region, as expected, but there is no plateau, meaning that the strain transfer from the structure towards the fiber core is not complete. Preliminary studies have shown that the bonding length should be sufficient for a complete strain transfer, suggesting again that further investigation on the bonding process inside the channel is required.

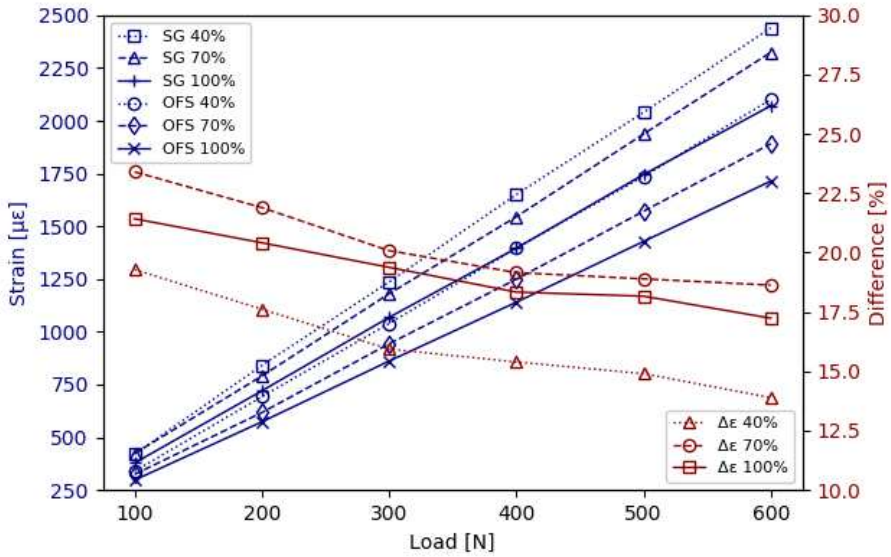

Fig. 5. Experimental results. Maximum strain measured by SG and OFS for different load and filling density values.

Fig. 7 shows the results of a numerical simulation performed with Abaqus/CAE for the case of 40% filling density and 300 N of applied force. The first observation is that the strain distribution along the core of the OFS has a periodicity depending on the triangles filling pattern intersecting the channel. However, Fig. 6 clearly showed that this periodicity was not present in the experimental measurements. The reason can be found in the interrogator resolution which in this case was set to 10 mm (lower values increases the noise and leads to measurement instabilities).

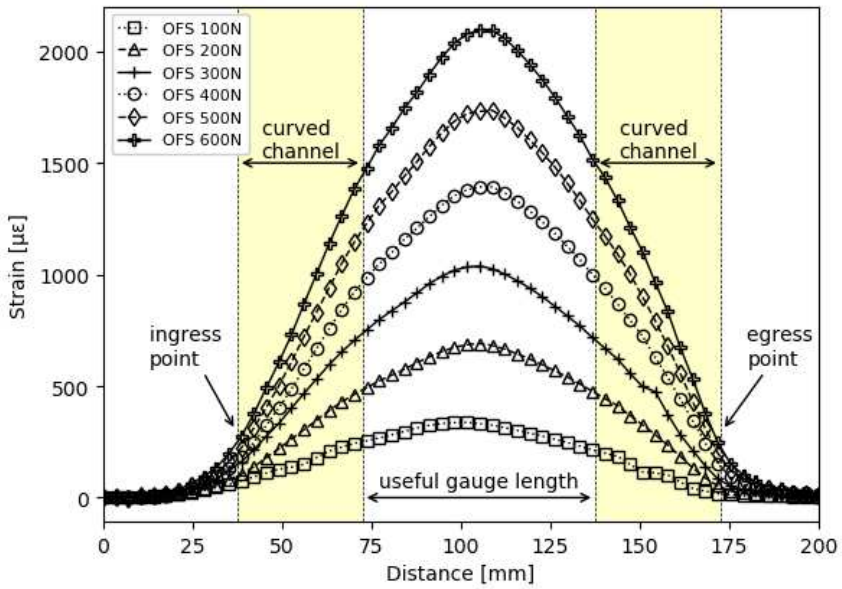

Fig. 6. Distributed measurement results at 40% of filling density.

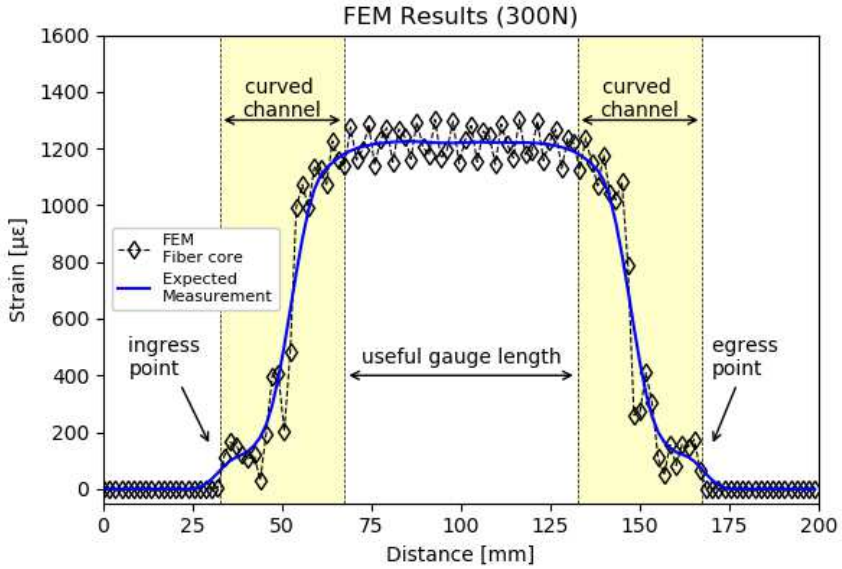

Fig. 7. Numerical results at 300N and 40% filling density.

This can be simulated applying a boxcar filter with 10 mm of width to the strain profile, leading to the blue solid line of Fig. 7. This is in line with the experimental data even if the numerical results show a clear plateau in the central region as if a complete

strain transfer is achieved. This discrepancy with respect to the numerical data can be related to the tie constraint applied in Abaqus/CAE. Indeed, the tie constraints between the OFS and the adhesive, and between the adhesive and the channel must be considered as ideal in the numerical model, therefore increasing the strain transfer efficiency. This point suggests that in future studies, the numerical model should also take into account this effect.

In conclusion, considering the strain values provided by the SG as a reference, since they are bonded on the outer shell of the specimen where there are no voids due to the filling pattern and the strain field is almost homogenous, further studies should clarify the difference with respect the OFS values. Therefore, longer specimens and hence longer bonding lengths will be considered to guarantee a complete strain transfer. The optimal channel size and the adhesive injection are also key elements which need further investigation.

References

1. Farrar, C.R., Worden, K.: An introduction to structural health monitoring. Philosophical Transactions of the Royal Society A: Mathematical, Physical and Engineering Sciences. 365, 303–315 (2007). https://doi.org/10.1098/rsta.2006.1928.
2. Huang, S.H., Liu, P., Mokasdar, A., Hou, L.: Additive manufacturing and its societal impact: a literature review. Int J Adv Manuf Technol. 67, 1191–1203 (2013). https://doi.org/10.1007/s00170-012-4558-5.
3. Wong, K.V., Hernandez, A.: A Review of Additive Manufacturing. ISRN Mechanical Engineering. 2012, 1–10 (2012). https://doi.org/10.5402/2012/208760.
4. Vaezi, M., Yang, S.: Extrusion-based additive manufacturing of PEEK for biomedical applications. Virtual and Physical Prototyping. 10, 123–135 (2015). https://doi.org/10.1080/17452759.2015.1097053.
5. Leal-Junior, A., Casas, J., Marques, C., Pontes, M., Frizera, A.: Application of Additive Layer Manufacturing Technique on the Development of High Sensitive Fiber Bragg Grating Temperature Sensors. Sensors. 18, 4120 (2018). https://doi.org/10.3390/s18124120.
6. Camposeo, A., Persano, L., Farsari, M., Pisignano, D.: Additive Manufacturing: Applications and Directions in Photonics and Optoelectronics. Advanced Optical Materials. 7, 1800419 (2019). https://doi.org/10.1002/adom.201800419.
7. Prakash, K.S., Nancharaih, T., Rao, V.V.S.: Additive Manufacturing Techniques in Manufacturing -An Overview. Materials Today: Proceedings. 5, 3873–3882 (2018). https://doi.org/10.1016/j.matpr.2017.11.642.
8. Reggiani Manzo, N., T. Callado, G., M.B. Cordeiro, C., M. Vieira Jr., L.C.: Embedding optical Fiber Bragg Grating (FBG) sensors in 3D printed casings. Optical Fiber Technology. 53, 102015 (2019). https://doi.org/10.1016/j.yofte.2019.102015.
9. Kousiatza, C., Karalekas, D.: In-situ monitoring of strain and temperature distributions during fused deposition modeling process. Materials & Design. 97, 400–406 (2016). https://doi.org/10.1016/j.matdes.2016.02.099.

10. Kantaros, A., Karalekas, D.: Fiber Bragg grating based investigation of residual strains in ABS parts fabricated by fused deposition modeling process. Materials & Design. 50, 44–50 (2013). https://doi.org/10.1016/j.matdes.2013.02.067.
11. Lehmhus, D., Aumund-Kopp, C., Petzoldt, F., Godlinski, D., Haberkorn, A., Zöllmer, V., Busse, M.: Customized Smartness: A Survey on Links between Additive Manufacturing and Sensor Integration. Procedia Technology. 26, 284–301 (2016). https://doi.org/10.1016/j.protcy.2016.08.038.
12. Allevi, G., Capponi, L., Castellini, P., Chiariotti, P., Docchio, F., Freni, F., Marsili, R., Martarelli, M., Montanini, R., Pasinetti, S., Quattrocchi, A., Rossetti, R., Rossi, G., Sansoni, G., Tomasini, E.P.: Investigating Additive Manufactured Lattice Structures: A Multi-Instrument Approach. IEEE Trans. Instrum. Meas. 69, 2459–2467 (2020). https://doi.org/10.1109/TIM.2019.2959293.
13. Di Sante, R.: Fibre optic sensors for structural health monitoring of aircraft composite structures: recent advances and applications. Sensors. 15, 18666–18713 (2015). https://doi.org/10.3390/s150818666.
14. Di Sante, R., Donati, L., Troiani, E., Proli, P.: Evaluation of bending strain measurements in a composite sailboat bowsprit with embedded fibre Bragg gratings. Measurement. 54, 106–117 (2014). https://doi.org/10.1016/j.measurement.2014.04.019.
15. Zubel, M.G., Sugden, K., Webb, D.J., Sáez-Rodríguez, D., Nielsen, K., Bang, O.: Embedding silica and polymer fibre Bragg gratings (FBG) in plastic 3D-printed sensing patches. Presented at the SPIE Photonics Europe , Brussels, Belgium April 27 (2016). https://doi.org/10.1117/12.2228753.
16. Bastianini, F., Di Sante, R., Falcetelli, F., Marini, D., Bolognini, G.: Optical fiber sensing cables for Brillouin-based distributed measurements. Sensors. 19, 5172 (2019). https://doi.org/10.3390/s19235172.
17. Leal-Junior, A.G., Marques, C., Ribeiro, M.R.N., Pontes, M.J., Frizera, A.: FBG-Embedded 3-D Printed ABS Sensing Pads: The Impact of Infill Density on Sensitivity and Dynamic Range in Force Sensors. IEEE Sensors J. 18, 8381–8388 (2018). https://doi.org/10.1109/JSEN.2018.2866689.
18. Zelený, R., Včelák, J.: Strain Measuring 3D Printed Structure with Embedded Fibre Bragg Grating. Procedia Engineering. 168, 1338–1341 (2016). https://doi.org/10.1016/j.proeng.2016.11.367.
19. Falcetelli, F., Rossi, L., Di Sante, R., Bolognini, G.: Strain Transfer in Surface-Bonded Optical Fiber Sensors. Sensors. 20, 3100 (2020). https://doi.org/10.3390/s20113100.
20. LeBlanc, M., Guemes, A., Othonos, A., Huang, S.Y., Ohn, M., Measures, R.M.: Distributed strain measurement based on a fiber Bragg grating and its reflection spectrum analysis. Opt. Lett. 21, 1405 (1996). https://doi.org/10.1364/OL.21.001405.
21. Zarbakhsh, J., Iravani, A., Amin-Akhlaghi, Z.: Sub-modeling Finite Element Analysis of 3D printed structures. In: 2015 16th International Conference on Thermal, Mechanical and Multi-Physics Simulation and Experiments in Microelectronics and Microsystems. pp. 1–4. IEEE, Budapest, Hungary (2015). https://doi.org/10.1109/EuroSimE.2015.7103095.
22. Guemes, J.A., Menéndez, J.M.: Response of Bragg grating fiber-optic sensors when embedded in composite laminates. Composites Science and Technology. 62, 959–966 (2002). https://doi.org/10.1016/S0266-3538(02)00010-6.
23. Corning Incorporated: SMF-28® Ultra and SMF-28® Ultra 200 Optical Fibers. (2019).